Biophysical Journal, Volume *114*

Supplemental Information

Vinculin Force-Sensitive Dynamics at Focal Adhesions Enable Effective Directed Cell Migration

Katheryn E. Rothenberg, David W. Scott, Nicolas Christoforou, and Brenton D. Hoffman

Supporting Tables:

Table S1. P-values from Steel-Dwass Test for FRET Data in Figures 2, 4, and S7			
VinTS	VinTS A50I	<0.0001	***
VinTS	VinTS I997A	<0.0001	***
VinTS	VinTS + Y	<0.0001	***
VinTS	VinTS A50I + Y	1.0000	NS
VinTS	VinTS I997A + Y	<0.0001	***
VinTS	VinTS + Lat A	0.9853	NS
VinTS	VinTS A50I + Lat A	<0.0001	***
VinTS A50I	VinTS I997A	<0.0001	***
VinTS A50I	VinTS + Y	0.0002	***
VinTS A50I	VinTS A50I + Y	0.0036	**
VinTS A50I	VinTS I997A + Y	<0.0001	***
VinTS A50I	VinTS + Lat A	0.0043	**
VinTS A50I	VinTS A50I + LatA	<0.0001	***
VinTS I997A	VinTS + Y	0.4394	NS
VinTS I997A	VinTS A50I + Y	<0.0001	***
VinTS I997A	VinTS I997A +Y	0.9429	NS
VinTS I997A	VinTS + LatA	<0.0001	***
VinTS I997A	VinTS A50I + LatA	<0.0001	***
VinTS + Y	VinTS A50I + Y	<0.0001	***
VinTS + Y	VinTS I997A + Y	0.9333	NS
VinTS + Y	VinTS + LatA	<0.0001	***
VinTS + Y	VinTS A50I + LatA	0.5914	NS
VinTS A50I + Y	VinTS I997A + Y	<0.0001	***
VinTS A50I + Y	VinTS + LatA	0.9961	NS
VinTS A50I + Y	VinTS A50I + LatA	<0.0001	***
VinTS I997A + Y	VinTS + LatA	<0.0001	***
VinTS I997A + Y	VinTS A50I + LatA	<0.0001	***
VinTS + LatA	VinTS A50I + LatA	<0.0001	***

Table S2. P-values from Steel-Dwass Test for FRAP Data in Figures 3 and 5					
		Half-Time		Mobile Fraction	
VinTS	VinTS A50I	0.0044	**	0.0013	**
VinTS	VinTS I997A	0.9839	NS	0.3994	NS
VinTS	VinTS + Y	0.0174	*	0.9120	NS
VinTS	VinTS A50I + Y	0.0057	**	0.0008	***
VinTS	VinTS I997A + Y	<0.0001	***	0.2171	NS
VinTS A50I	VinTS I997A	0.1842	NS	<0.0001	***
VinTS A50I	VinTS + Y	1.0000	NS	0.0002	***
VinTS A50I	VinTS A50I + Y	0.8863	NS	0.9997	NS
VinTS A50I	VinTS I997A + Y	0.2414	NS	<0.0001	***
VinTS I997A	VinTS + Y	0.4220	NS	0.9324	NS
VinTS I997A	VinTS A50I + Y	0.1046	NS	<0.0001	***
VinTS I997A	VinTS I997A +Y	0.0126	*	0.9976	NS
VinTS + Y	VinTS A50I + Y	0.9109	NS	0.0007	***
VinTS + Y	VinTS I997A + Y	0.2532	NS	0.7659	NS
VinTS A50I + Y	VinTS I997A + Y	0.8767	NS	<0.0001	***

Supporting Figures:

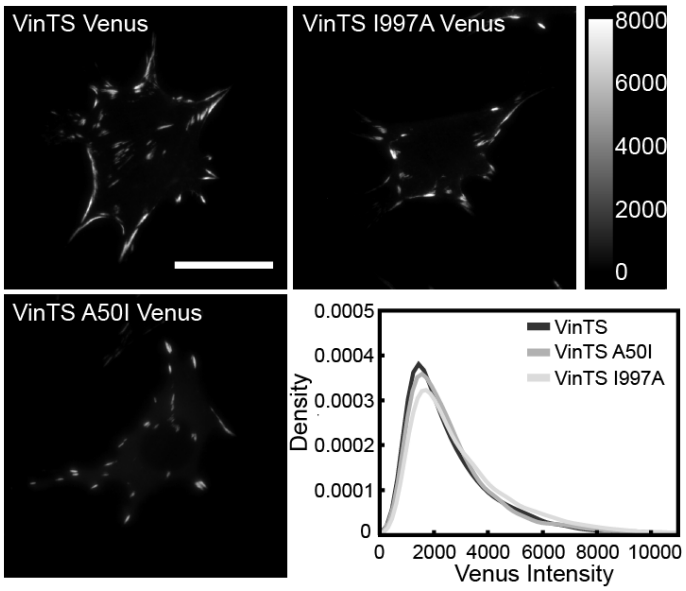

Figure S1. Vinculin expression at FAs. After viral transduction, MEFs were sorted by intensity using flow cytometry. We matched vinculin expression at FAs between the different mutant-expressing cells using the acceptor imaging channel, which is proportional to vinculin concentration. Images show three representative cells in the acceptor imaging channel. The probability density plot compares the intensities of all FAs imaged in each cell line (n = 93, 82, and 79 cells, from 4 independent experiments). No difference between groups was detected using the Kolmogorov–Smirnov test.

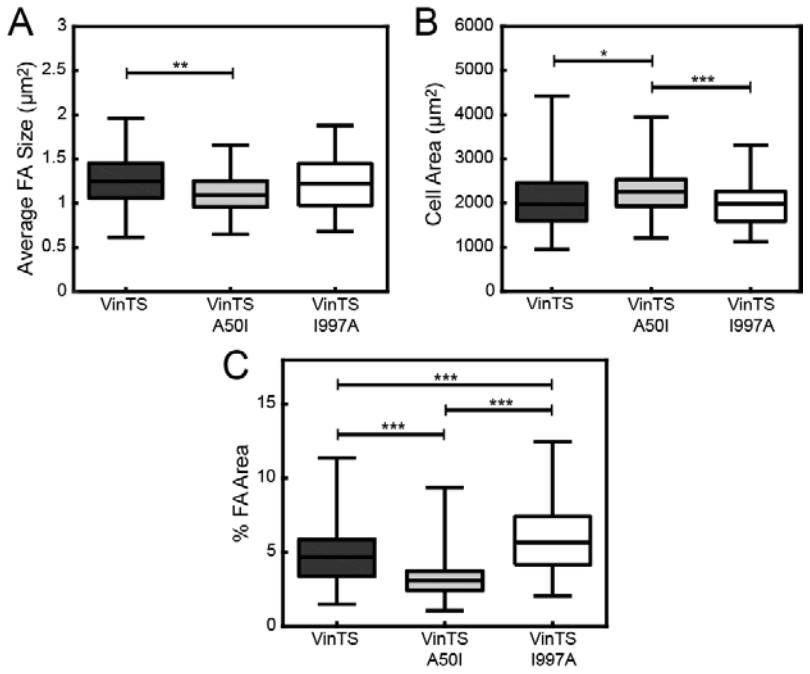

Figure S2. Cell and focal adhesion properties in MEFs expressing VinTS or the mutant constructs VinTS A50I or VinTS I997A. (A) Box-whisker plots of average FA size in cells expressing the vinculin tension sensor constructs show that VinTS A50I MEFs have smaller FAs on average, while VinTS I997A MEFs have slightly larger FAs on average than VinTS MEFs. (B) Box-whisker plots of average cell area. VinTS A50I MEFs are slightly larger than VinTS and VinTS I997A MEFs on average. (C) Box-whisker plots of percent of cell area occupied by FAs (% FA area). VinTS I997A MEFs have the highest percentage area occupied by FAs, while VinTS A50I MEFs have the lowest percentage area occupied by FAs, compared with VinTS MEFs. n = 93, 82, and 79 cells, respectively, from 4 independent experiments. Differences between groups was detected using Tukey's HSD test. (* = $p < 0.05$, ** = $p < 0.01$, *** = $p < 0.001$)

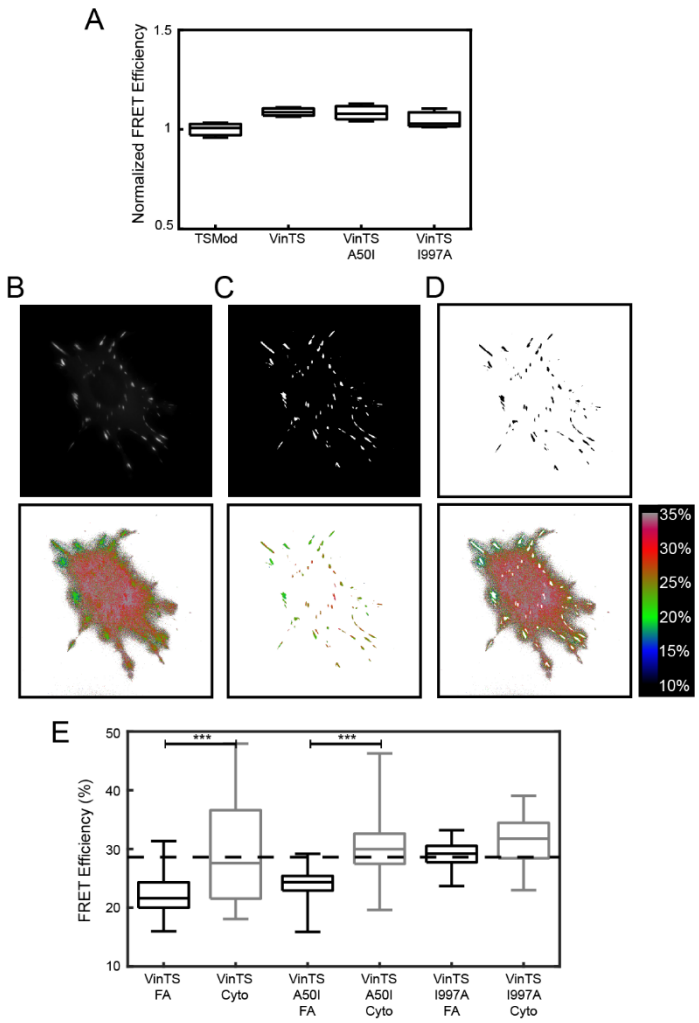

Figure S3. Vinculin bears no load in solution or in the cytosol. (A) Box-whisker plots of FRET efficiency as measured using spectrofluorimetry of the various vinculin tension sensor constructs in solution, normalized to the average TSMod FRET efficiency. There is no significant difference between any of the tension sensor constructs and TSMod, which cannot bear load; therefore, none of the vinculin variants bear load in solution. n = 3. (B) Representative VinTS A50I MEF in the acceptor channel (top panel) and its calculated FRET efficiencies (bottom panel). (C) Binary FA mask generated based on acceptor channel (top panel) and applied to calculated FRET efficiency (bottom panel). (D) Binary inverted FA mask used to eliminate FAs (top panel) and applied to calculated FRET efficiency (bottom panel). (E) Box-whisker plots of average FRET efficiency either within FAs (black) or in the cytosol outside FAs (gray) for each of the vinculin tension sensor variants (n = 79, 85, and 50 cells, respectively, from 7 independent experiments) compared to previously established zero-load (dotted line). For all the vinculin variants, the average load in the cytosol is zero. Differences between groups was detected using the Steel-Dwass test. (* = $p < 0.05$, *** = $p < 0.001$)

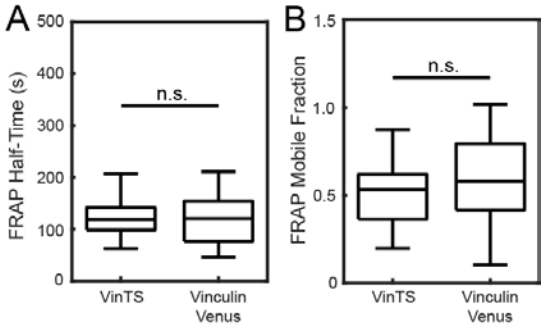

Figure S4. VinTS turnover post-FRET imaging is indistinguishable from turnover of Vinculin tagged with Venus on the C-terminus without prior FRET imaging. FRAP half-time (A) and mobile fraction (B) are not different between VinTS and Vinculin-Venus. This indicates that neither the insertion of the tension sensor module nor the use of FRET imaging impact vinculin turnover (n = 12 and 15 FAs, respectively, from three independent experiments). VinTS FRAP half-time and mobile fraction in this data set were found to be statistically indistinguishable from the VinTS FRAP half-time and mobile fraction presented in Fig. 3.

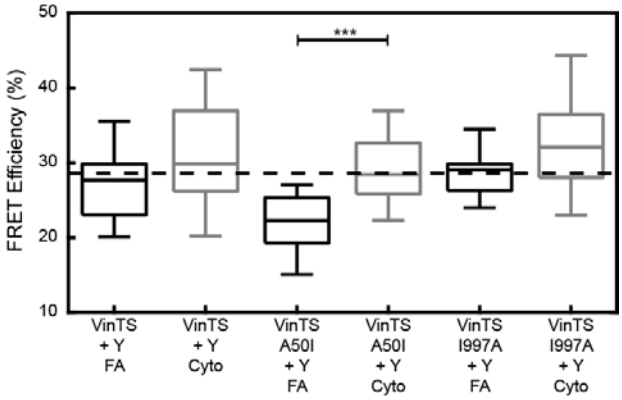

Figure S5. Vinculin bears no load in the cytosol after treatment with Y-27632. Box-whisker plots of average FRET efficiency either within FAs (black) or in the cytosol outside FAs (gray) for each of the vinculin tension sensor variants (n = 24, 32, and 30 cells, respectively, from 4 independent experiments) compared to previously established zero-load (dotted line). For all the vinculin variants, the average load in the cytosol is zero. Differences between groups was detected using the Steel-Dwass test. (*** = $p < 0.001$)

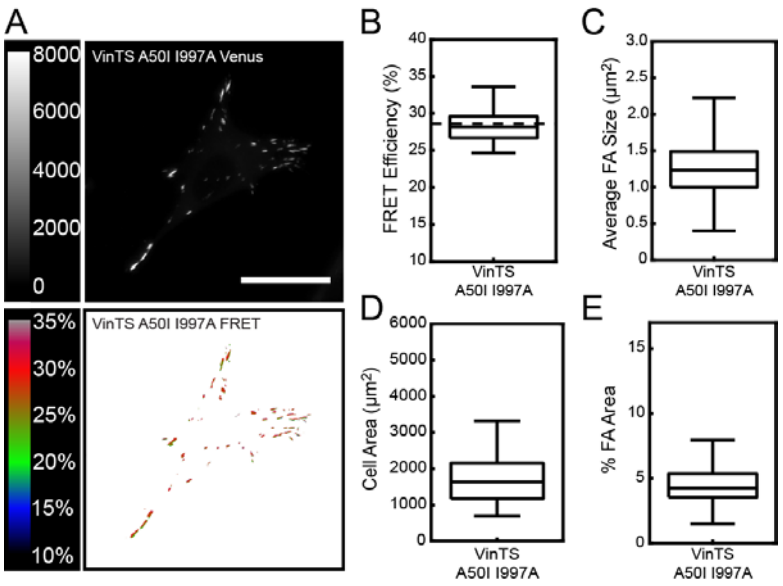

Figure S6. VinTS A50I requires actin binding to be loaded. (A) Representative acceptor (top) and masked FRET efficiency (bottom) images of single Vinc -/- MEFs transiently expressing VinTS A50I I997A, following standard Lipofectamine 2000 protocols. Scale bar = 30 μm. (B) Box-whisker plot of cell-averaged FRET efficiency, which is indistinguishable from established zero load (dotted line). (C) Box-whisker plot of average FA size, which is similar to VinTS. (D) Box-whisker plot of cell area, which is smaller than cells expressing the other vinculin tension sensor variants. (E) Box-whisker plot of percent FA area, which is similar to VinTS. n = 49 cells from 3 independent experiments.

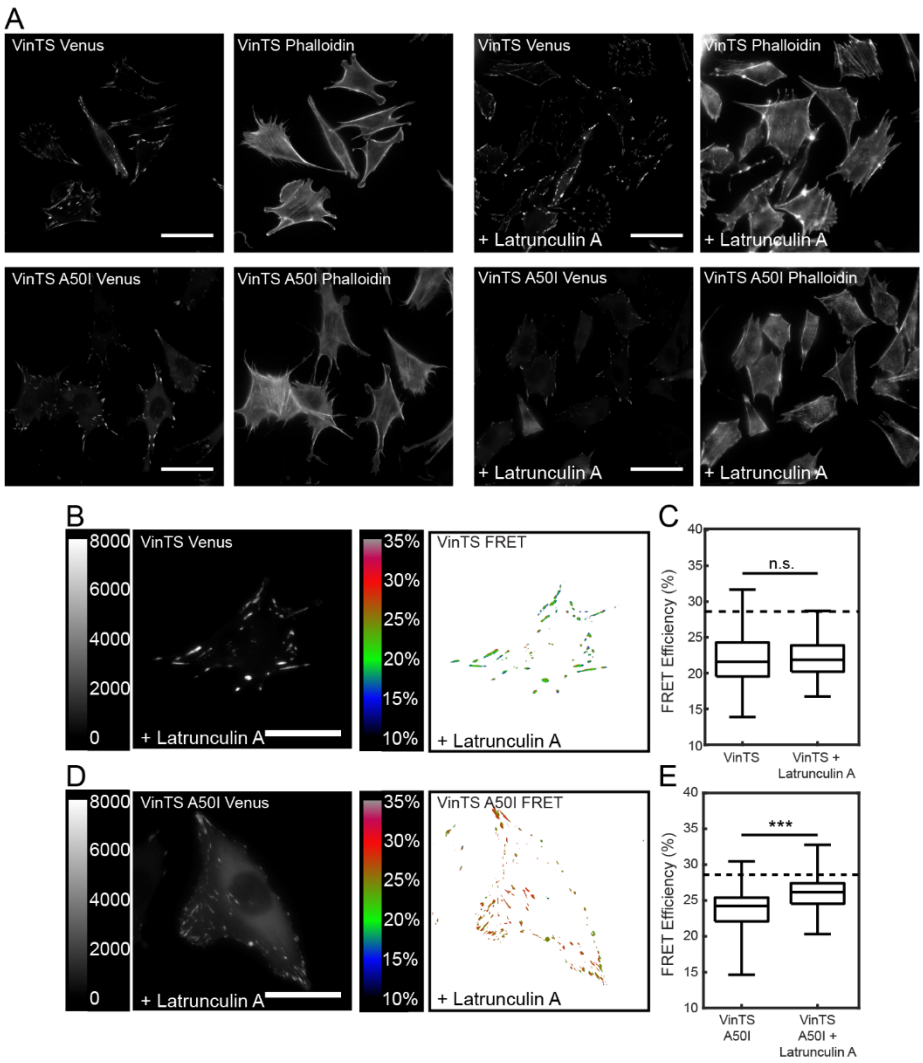

Figure S7. Vinculin A50I is partially loaded via actin polymerization. (A) VinTS and VinTS A50I MEFs untreated or treated with 250 nM latrunculin A for 20 minutes, fixed in 4% paraformaldehyde, and stained with phalloidin 647. This dose of latrunculin A was chosen to prevent actin polymerization but maintain existing stress fibers. (B) Representative acceptor (left) and masked FRET efficiency (right) image of single VinTS MEF treated with latrunculin A. Scale bar = 30 μm. (C) Box-whisker plot of cell averaged FRET efficiency (n = 150 and 62 cells, respectively, from 3 independent experiments) compared to previously established zero-load (dotted line). (D) Representative acceptor (left) and masked FRET efficiency (right) image of single VinTS A50I MEF treated with latrunculin A. Scale bar = 30 μm. (E) Box-whisker plot of cell averaged FRET efficiency (n = 166 and 84 cells, respectively, from 3 independent experiments) compared to previously established zero-load (dotted line). A significant loss of vinculin A50I load was detected. Note that the FRET data for untreated groups in C and E is reprinted from Fig. 2.

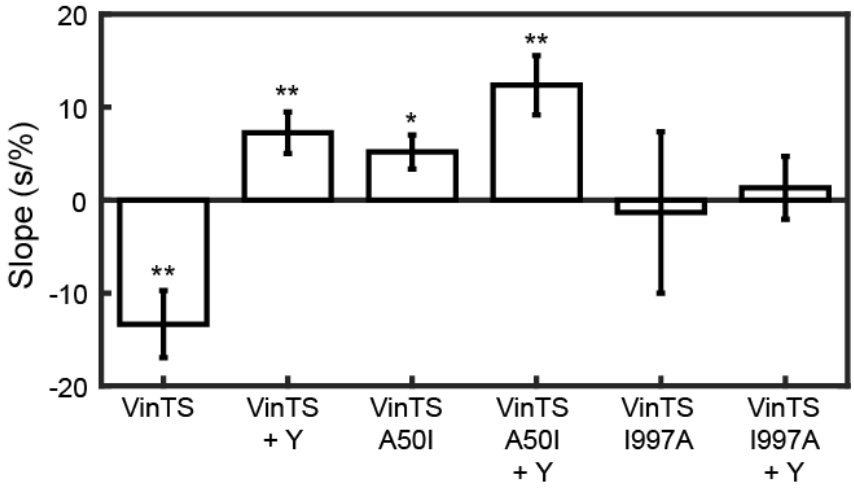

Figure S8. Regression slopes calculated for FRET-FRAP assay. Related to Figure 5. A least-squares linear regression was fit to the FRAP half-time and FRET efficiency data for each construct. Bars represent slope and error bars represent standard error of the regression slope. All slopes are statistically different from zero except for VinTS I997A and VinTS I997A + Y-27632. P-values indicate the results of a t-test comparing the regression slope to zero. (* = $p < 0.05$, ** = $p < 0.01$)

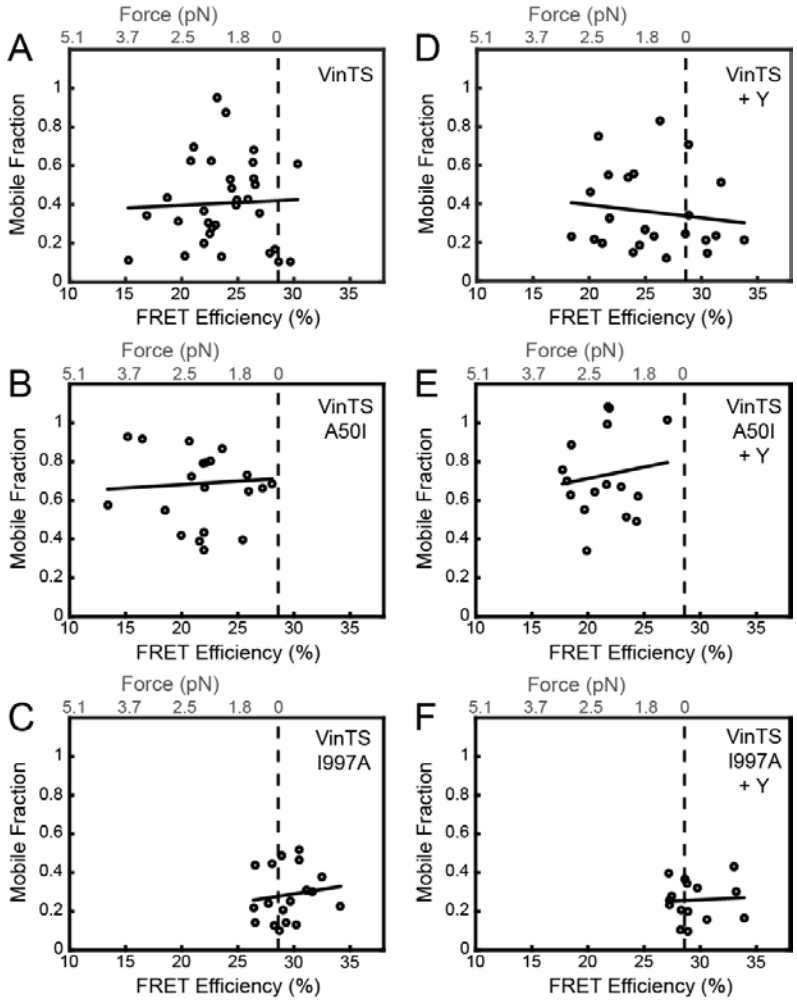

Figure S9. Novel FRET-FRAP assay shows that mobile fraction is force-insensitive. (A-F) No detectable correlation between FRAP mobile fraction and FRET efficiency was observed for any of the expressed constructs or treatments.

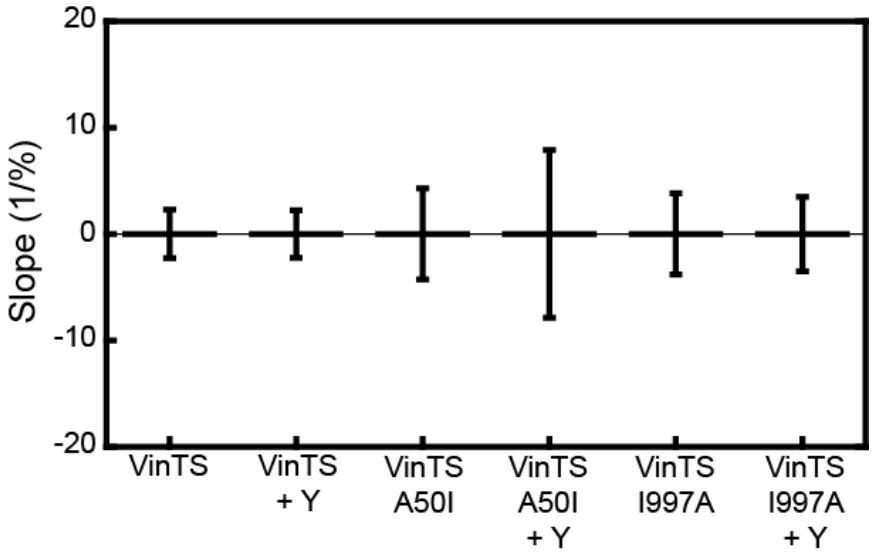

Figure S10. Regression slopes calculated for mobile fraction vs. FRET efficiency. Related to Figure S9. A least-squares linear regression was fit to the FRAP mobile fraction and FRET efficiency data for each construct. Bars represent slope and error bars represent standard error of the regression slope. None of the slopes are statistically different from zero, as determined by a t-test comparing the regression slope to zero.

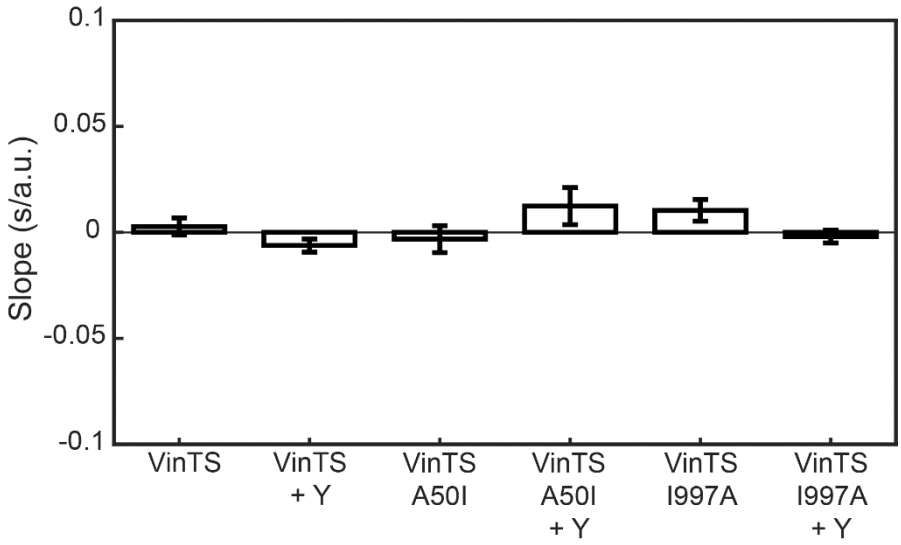

Figure S11. Regression slopes calculated for FRAP half-time vs. Venus mean intensity at the single FA. Bars represent slope and error bars represent standard error of the regression slope. None of the slopes are statistically different from zero, as determined by a t-test comparing the regression slope to zero.

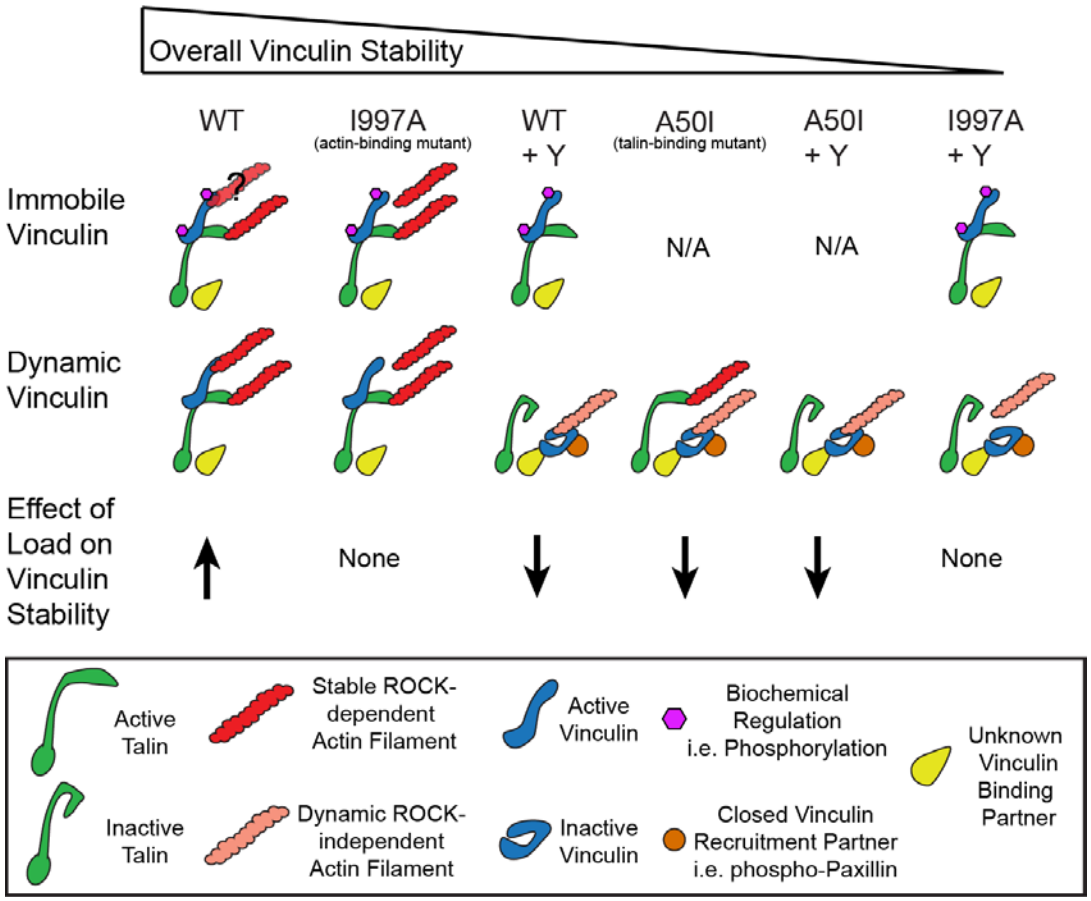

Figure S12. Schematic of mechanical states of vinculin, ordered from most stable to least stable (left to right). i) We find that a large population of WT vinculin at FAs is immobile. Based on previous work, we suggest that vinculin is in the open conformation and held in this immobile state by biochemical regulation, such as phosphorylation at sites Y100 and Y1065 (1). The dynamic WT vinculin population is bound to both talin and actin, with increased load across vinculin leading to further stabilization, which we refer to as the force-stabilized state. ii) Vinculin I997A still has a large immobile population of vinculin, making it clear that binding to actin is not necessary for the existence of this state. There is also a dynamic population, though its turnover rate is insensitive to vinculin load. iii) Short-term ROCK inhibition does not affect the amount of WT vinculin in the immobile state. The dynamic population of WT vinculin under ROCK inhibition is less stable and is in the force-destabilized state. ROCK inhibition leads to the unloading of talin (2, 3). This likely prevents the exposure of cryptic binding sites for vinculin, and leads to vinculin binding to an alternative partner. Due to similarities between this state and vinculin A50I, we suggest that phosphorylated paxillin recruits vinculin to this alternative binding partner, which may be another site on talin or another FA protein (4). Notably, a force-sensitive interaction between vinculin and actinin has also been demonstrated (5). iv) Vinculin A50I does not exhibit an appreciable immobile fraction, consistent with its reduced affinity for talin, enhanced head-tail inhibition, and propensity to remain in a closed conformation at FAs (4, 6). When under load, it forms the force-destabilized state. Vinculin A50I has previously been reported to interact with phosphorylated paxillin, suggesting a key role in recruitment to the FA (4). v) Vinculin A50I is unaffected by ROCK inhibition. This is consistent with the idea that vinculin A50I localization to FAs is not associated with loaded talin, but rather is loaded via actin polymerization. vi) Vinculin I997A under ROCK inhibition also exhibits a large population of vinculin in the immobile state. It is not likely that vinculin I997A binds to talin when ROCK is inhibited, suggesting it interacts with an alternative binding partner. We propose that this is the least stable state as it forms the fewest number of physical connections. We also note for all the constructs that the percentage of vinculin in the immobile state is not correlated with vinculin load and not affected by ROCK inhibition, suggesting mechanical loading does not a play a role in the initiation or maintenance of this state. This raises the possibility that this state may be unloaded and not bound to actin. This ambiguity has been noted in the depiction of the actin filament associated with this state.

Supporting Movie Stills:

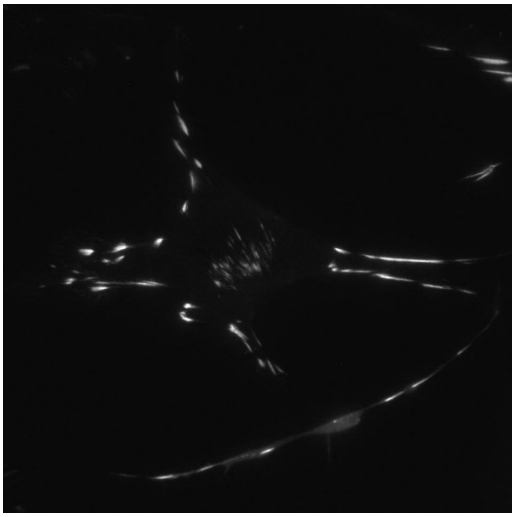

Movie S1. VinTS MEF FRAP. Movie shows fluorescent imaging of VinTS at FAs in the Venus imaging channel. A single FA is bleached, and recovery is monitored. Images were taken every 5 seconds for 5.5 minutes. Photobleaching occurs in the 5th frame.

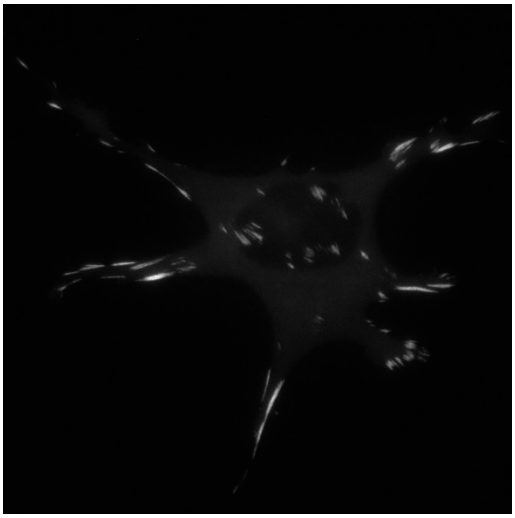

Movie S2. VinTS A50I MEF FRAP. Movie shows fluorescent imaging of VinTS A50I at FAs in the Venus imaging channel. A single FA is bleached, and recovery is monitored. Images were taken every 5 seconds for 5.5 minutes. Photobleaching occurs in the 5th frame.

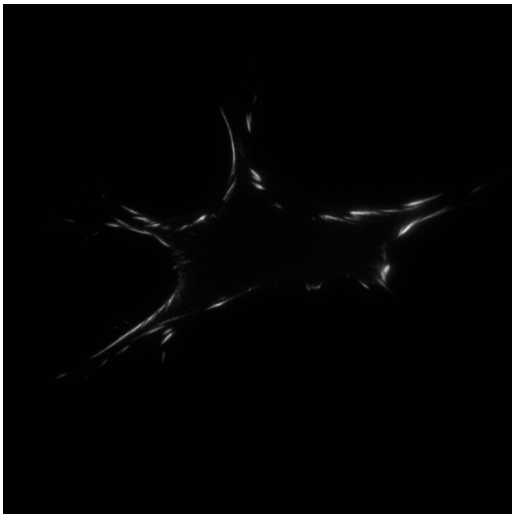

Movie S3. VinTS I997A MEF FRAP. Movie shows fluorescent imaging of VinTS I997A at FAs in the Venus imaging channel. A single FA is bleached, and recovery is monitored. Images were taken every 5 seconds for 5.5 minutes. Photobleaching occurs in the 5th frame.

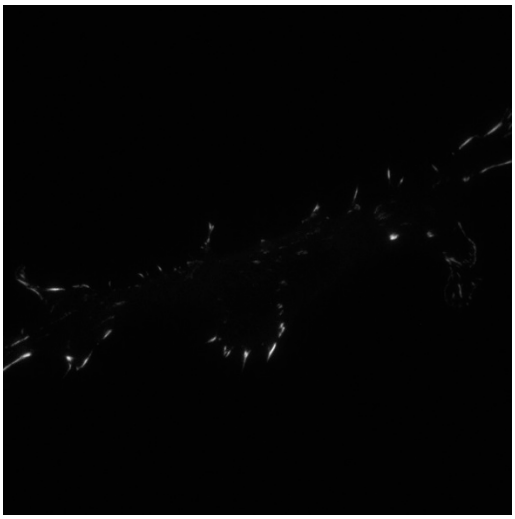

Movie S4. VinTS MEF FRAP + Y-27632. Movie shows fluorescent imaging of VinTS at FAs in the Venus imaging channel after treatment with Y-27632. A single FA is bleached, and recovery is monitored. Images were taken every 5 seconds for 5.5 minutes. Photobleaching occurs in the 5th frame.

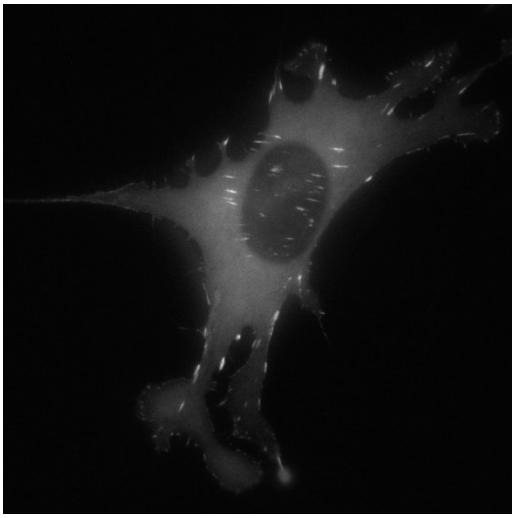

Movie S5. VinTS A50I MEF FRAP + Y-27632. Movie shows fluorescent imaging of VinTS A50I at FAs in the Venus imaging channel after treatment with Y-27632. A single FA is bleached, and recovery is monitored. Images were taken every 5 seconds for 5.5 minutes. Photobleaching occurs in the 5th frame.

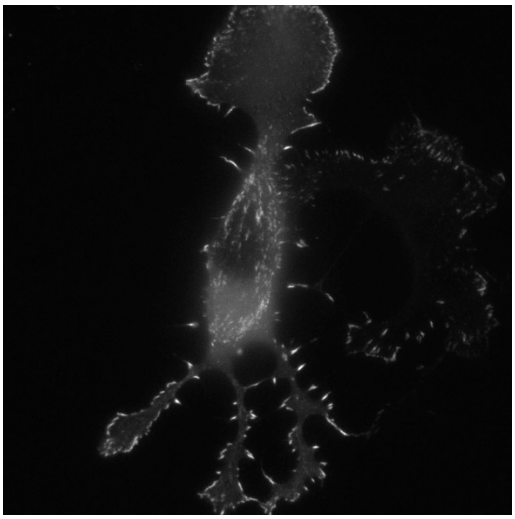

Movie S6. VinTS I997A MEF FRAP + Y-27632. Movie shows fluorescent imaging of VinTS I997A at FAs in the Venus imaging channel after treatment with Y-27632. A single FA is bleached, and recovery is monitored. Images were taken every 5 seconds for 5.5 minutes. Photobleaching occurs in the 5th frame.

Supporting References:

1. Auernheimer, V., L. A. Lautscham, M. Leidenberger, O. Friedrich, B. Kappes, B. Fabry, and W. H. Goldmann. 2015. Vinculin phosphorylation at residues Y100 and Y1065 is required for cellular force transmission. J Cell Sci 128:3435-3443.
2. Austen, K., P. Ringer, A. Mehlich, A. Chrostek-Grashoff, C. Kluger, C. Klingner, B. Sabass, R. Zent, M. Rief, and C. Grashoff. 2015. Extracellular rigidity sensing by talin isoform-specific mechanical linkages. Nat Cell Biol 17:1597-1606.
3. Kumar, A., M. Ouyang, K. Van den Dries, E. J. McGhee, K. Tanaka, M. D. Anderson, A. Groisman, B. T. Goult, K. I. Anderson, and M. A. Schwartz. 2016. Talin tension sensor reveals novel features of focal adhesion force transmission and mechanosensitivity. J Cell Biol 213:371-383.
4. Case, L. B., M. A. Baird, G. Shtengel, S. L. Campbell, H. F. Hess, M. W. Davidson, and C. M. Waterman. 2015. Molecular mechanism of vinculin activation and nanoscale spatial organization in focal adhesions. Nat Cell Biol 17:880-892.
5. Le, S., X. Hu, M. Yao, H. Chen, M. Yu, X. Xu, N. Nakazawa, F. M. Margadant, M. P. Sheetz, and J. Yan. 2017. Mechanotransmission and Mechanosensing of Human alpha-Actinin 1. Cell Rep 21:2714-2723.
6. Cohen, D. M., B. Kutscher, H. Chen, D. B. Murphy, and S. W. Craig. 2006. A conformational switch in vinculin drives formation and dynamics of a talin-vinculin complex at focal adhesions. J Biol Chem 281:16006-16015.